EUROPEAN ORGANISATION FOR NUCLEAR RESEARCH

CERN-PPE/95-193
December 21,1995

Search for a Narrow Resonance in Z^0 Decays into Hadrons and Isolated Photons

The OPAL Collaboration

Abstract

A search for the hadronic decay of a hypothetical resonance S^0 in the process $e^+e^- \to \gamma$ + hadrons at Z^0 energies is reported. Particular care is taken to optimise the sensitivity to a scalar resonance decaying into bottom quarks, as expected for Higgs production, $e^+e^- \to Z^0 \to H^0\gamma$ with $H^0 \to b\bar{b}$, in the Standard Model or some of its extensions. No evidence for such a resonance is observed in a sample of about 5 million produced Z^0's. The results are interpreted in terms of models of non-standard Higgs production. An update of a search for a resonance produced in association with hadrons and the subsequent resonance decay into two photons is also presented.

Submitted to Zeitschrift für Physik C.

The OPAL Collaboration

G. Alexander[23], J. Allison[16], N. Altekamp[5], K. Ametewee[25], K.J. Anderson[9], S. Anderson[12], S. Arcelli[2], S. Asai[24], D. Axen[29], G. Azuelos[18,a], A.H. Ball[17], E. Barberio[26], R.J. Barlow[16], R. Bartoldus[3], J.R. Batley[5], G. Beaudoin[18], J. Bechtluft[14], C. Beeston[16], T. Behnke[8], A.N. Bell[1], K.W. Bell[20], G. Bella[23], S. Bentvelsen[8], P. Berlich[10], S. Bethke[14], O. Biebel[14], V. Blobel[8], I.J. Bloodworth[1], J.E. Bloomer[1], P. Bock[11], H.M. Bosch[11], M. Boutemeur[18], B.T. Bouwens[12], S. Braibant[12], P. Bright-Thomas[25], R.M. Brown[20], H.J. Burckhart[8], C. Burgard[27], R. Bürgin[10], P. Capiluppi[2], R.K. Carnegie[6], A.A. Carter[13], J.R. Carter[5], C.Y. Chang[17], C. Charlesworth[6], D.G. Charlton[1,b], D. Chrisman[4], S.L. Chu[4], P.E.L. Clarke[15], S.G. Clowes[16], I. Cohen[23], J.E. Conboy[15], O.C. Cooke[16], M. Cuffiani[2], S. Dado[22], C. Dallapiccola[17], G.M. Dallavalle[2], C. Darling[31], S. De Jong[12], L.A. del Pozo[8], M.S. Dixit[7], E. do Couto e Silva[12], E. Duchovni[26], G. Duckeck[8], I.P. Duerdoth[16], J.E.G. Edwards[16], P.G. Estabrooks[6], H.G. Evans[9], M. Evans[13], F. Fabbri[2], P. Fath[11], F. Fiedler[12], M. Fierro[2], H.M. Fischer[3], R. Folman[26], D.G. Fong[17], M. Foucher[17], H. Fukui[24], A. Fürtjes[8], P. Gagnon[7], A. Gaidot[21], J.W. Gary[4], J. Gascon[18], S.M. Gascon-Shotkin[17], N.I. Geddes[20], C. Geich-Gimbel[3], S.W. Gensler[9], F.X. Gentit[21], T. Geralis[20], G. Giacomelli[2], P. Giacomelli[4], R. Giacomelli[2], V. Gibson[5], W.R. Gibson[13], D.M. Gingrich[30,a], J. Goldberg[22], M.J. Goodrick[5], W. Gorn[4], C. Grandi[2], E. Gross[26], M. Gruwé[8], C. Hajdu[32], G.G. Hanson[12], M. Hansroul[8], M. Hapke[13], C.K. Hargrove[7], P.A. Hart[9], C. Hartmann[3], M. Hauschild[8], C.M. Hawkes[5], R. Hawkings[8], R.J. Hemingway[6], G. Herten[10], R.D. Heuer[8], M.D. Hildreth[8], J.C. Hill[5], S.J. Hillier[1], T. Hilse[10], P.R. Hobson[25], R.J. Homer[1], A.K. Honma[28,a], D. Horváth[32,c], R. Howard[29], R.E. Hughes-Jones[16], D.E. Hutchcroft[5], P. Igo-Kemenes[11], D.C. Imrie[25], A. Jawahery[17], P.W. Jeffreys[20], H. Jeremie[18], M. Jimack[1], A. Joly[18], M. Jones[6], R.W.L. Jones[8], U. Jost[11], P. Jovanovic[1], J. Kanzaki[24], D. Karlen[6], T. Kawamoto[24], R.K. Keeler[28], R.G. Kellogg[17], B.W. Kennedy[20], J. King[13], J. Kirk[29], S. Kluth[8], T. Kobayashi[24], M. Kobel[10], D.S. Koetke[6], T.P. Kokott[3], S. Komamiya[24], R. Kowalewski[8], T. Kress[11], P. Krieger[6], J. von Krogh[11], P. Kyberd[13], G.D. Lafferty[16], H. Lafoux[21], R. Lahmann[17], W.P. Lai[19], D. Lanske[14], J. Lauber[15], J.G. Layter[4], A.M. Lee[31], E. Lefebvre[18], D. Lellouch[26], J. Letts[2], L. Levinson[26], C. Lewis[15], S.L. Lloyd[13], F.K. Loebinger[16], G.D. Long[17], B. Lorazo[18], M.J. Losty[7], J. Ludwig[10], A. Luig[10], A. Malik[21], M. Mannelli[8], S. Marcellini[2], C. Markus[3], A.J. Martin[13], J.P. Martin[18], G. Martinez[17], T. Mashimo[24], W. Matthews[25], P. Mättig[3], W.J. McDonald[30], J. McKenna[29], E.A. Mckigney[15], T.J. McMahon[1], A.I. McNab[13], F. Meijers[8], S. Menke[3], F.S. Merritt[9], H. Mes[7], J. Meyer[27], A. Michelini[8], G. Mikenberg[26], D.J. Miller[15], R. Mir[26], W. Mohr[10], A. Montanari[2], T. Mori[24], M. Morii[24], U. Müller[3], B. Nellen[3], B. Nijjhar[16], R. Nisius[8], S.W. O'Neale[1], F.G. Oakham[7], F. Odorici[2], H.O. Ogren[12], N.J. Oldershaw[16], T. Omori[24], M.J. Oreglia[9], S. Orito[24], M. Palazzo[2], J. Pálinkás[33,d], F.M. Palmonari[2], J.P. Pansart[21], G. Pásztor[32], J.R. Pater[16], G.N. Patrick[20], M.J. Pearce[1], S. Petzold[27], P.D. Phillips[16], J.E. Pilcher[9], J. Pinfold[30], D.E. Plane[8], P. Poffenberger[28], B. Poli[2], A. Posthaus[3], H. Przysiezniak[30], D.L. Rees[1], D. Rigby[1], M.G. Rison[5], S.A. Robins[13], N. Rodning[30], J.M. Roney[28], E. Ros[8], A.M. Rossi[2], M. Rosvick[28], P. Routenburg[30], Y. Rozen[8], K. Runge[10], O. Runolfsson[8], D.R. Rust[12], R. Rylko[25], E.K.G. Sarkisyan[23], M. Sasaki[24], C. Sbarra[2], A.D. Schaile[8], O. Schaile[10], F. Scharf[3], P. Scharff-Hansen[8], P. Schenk[4], B. Schmitt[3], M. Schröder[8], H.C. Schultz-Coulon[10], M. Schulz[8], P. Schütz[3], J. Schwiening[3], W.G. Scott[20], T.G. Shears[16], B.C. Shen[4], C.H. Shepherd-Themistocleous[27], P. Sherwood[15], G.P. Siroli[2], A. Sittler[27], A. Skillman[15], A. Skuja[17], A.M. Smith[8], T.J. Smith[28], G.A. Snow[17], R. Sobie[28], S. Söldner-Rembold[10], R.W. Springer[30], M. Sproston[20], A. Stahl[3], M. Starks[12], K. Stephens[16], J. Steuerer[27], B. Stockhausen[3], D. Strom[19], F. Strumia[8], P. Szymanski[20], R. Tafirout[18],

H. Takeda[24], P. Taras[18], S. Tarem[22], M. Tecchio[8], N. Tesch[3], M. Thiergen[10], M.A. Thomson[8], E. von Törne[3], S. Towers[6], M. Tscheulin[10], E. Tsur[23], A.S. Turcot[9], M.F. Turner-Watson[8], P. Utzat[11], R. Van Kooten[12], G. Vasseur[21], M. Verzocchi[10], P. Vikas[18], M. Vincter[28], E.H. Vokurka[16], F. Wäckerle[10], A. Wagner[27], C.P. Ward[5], D.R. Ward[5], J.J. Ward[15], P.M. Watkins[1], A.T. Watson[1], N.K. Watson[7], P. Weber[6], P.S. Wells[8], N. Wermes[3], J.S. White[28], B. Wilkens[10], G.W. Wilson[27], J.A. Wilson[1], T. Wlodek[26], G. Wolf[26], S. Wotton[11], T.R. Wyatt[16], S. Xella[2], S. Yamashita[24], G. Yekutieli[26], K. Yoshimura[24], V. Zacek[18],

[1]School of Physics and Space Research, University of Birmingham, Birmingham B15 2TT, UK
[2]Dipartimento di Fisica dell' Università di Bologna and INFN, I-40126 Bologna, Italy
[3]Physikalisches Institut, Universität Bonn, D-53115 Bonn, Germany
[4]Department of Physics, University of California, Riverside CA 92521, USA
[5]Cavendish Laboratory, Cambridge CB3 0HE, UK
[6] Ottawa-Carleton Institute for Physics, Department of Physics, Carleton University, Ottawa, Ontario K1S 5B6, Canada
[7]Centre for Research in Particle Physics, Carleton University, Ottawa, Ontario K1S 5B6, Canada
[8]CERN, European Organisation for Particle Physics, CH-1211 Geneva 23, Switzerland
[9]Enrico Fermi Institute and Department of Physics, University of Chicago, Chicago IL 60637, USA
[10]Fakultät für Physik, Albert Ludwigs Universität, D-79104 Freiburg, Germany
[11]Physikalisches Institut, Universität Heidelberg, D-69120 Heidelberg, Germany
[12]Indiana University, Department of Physics, Swain Hall West 117, Bloomington IN 47405, USA
[13]Queen Mary and Westfield College, University of London, London E1 4NS, UK
[14]Technische Hochschule Aachen, III Physikalisches Institut, Sommerfeldstrasse 26-28, D-52056 Aachen, Germany
[15]University College London, London WC1E 6BT, UK
[16]Department of Physics, Schuster Laboratory, The University, Manchester M13 9PL, UK
[17]Department of Physics, University of Maryland, College Park, MD 20742, USA
[18]Laboratoire de Physique Nucléaire, Université de Montréal, Montréal, Quebec H3C 3J7, Canada
[19]University of Oregon, Department of Physics, Eugene OR 97403, USA
[20]Rutherford Appleton Laboratory, Chilton, Didcot, Oxfordshire OX11 0QX, UK
[21]CEA, DAPNIA/SPP, CE-Saclay, F-91191 Gif-sur-Yvette, France
[22]Department of Physics, Technion-Israel Institute of Technology, Haifa 32000, Israel
[23]Department of Physics and Astronomy, Tel Aviv University, Tel Aviv 69978, Israel
[24]International Centre for Elementary Particle Physics and Department of Physics, University of Tokyo, Tokyo 113, and Kobe University, Kobe 657, Japan
[25]Brunel University, Uxbridge, Middlesex UB8 3PH, UK
[26]Particle Physics Department, Weizmann Institute of Science, Rehovot 76100, Israel
[27]Universität Hamburg/DESY, II Institut für Experimental Physik, Notkestrasse 85, D-22607 Hamburg, Germany
[28]University of Victoria, Department of Physics, P O Box 3055, Victoria BC V8W 3P6, Canada
[29]University of British Columbia, Department of Physics, Vancouver BC V6T 1Z1, Canada
[30]University of Alberta, Department of Physics, Edmonton AB T6G 2J1, Canada

[31]Duke University, Dept of Physics, Durham, NC 27708-0305, USA
[32]Research Institute for Particle and Nuclear Physics, H-1525 Budapest, P O Box 49, Hungary
[33]Institute of Nuclear Research, H-4001 Debrecen, P O Box 51, Hungary

[a]Also at TRIUMF, Vancouver, Canada V6T 2A3
[b] Royal Society University Research Fellow
[c] Institute of Nuclear Research, Debrecen, Hungary
[d] Depart of Experimental Physics, Lajos Kossuth University, Debrecen, Hungary

1 Introduction

The mechanism of mass generation is one of the outstanding problems of the Standard Model. In its minimal version this is solved by introducing the Higgs boson H^0 [1], a fundamental scalar particle. Searches at LEP using the Bjorken process $Z^0 \to H^0 + Z^{*0}$ [2], where the off-shell Z^{*0} decays into a fermion pair, have found no evidence for such a Higgs boson and placed lower limits on its mass to $m_{H^0} > 64.5$ GeV [3]. An additional Z^0 decay mode into the Higgs particle is the loop decay $Z^0 \to H^0\gamma$ [4]. For Higgs masses smaller than about 60 GeV its Standard Model rate is strongly suppressed relative to the Bjorken process. However, for larger masses the radiative decay becomes the dominant mode of Z^0 decays into the Higgs. Furthermore, it is enhanced in some extensions of the Standard Model. For example, in Supersymmetric models its production rate can increase by up to a factor of three [5]. It has also been conjectured [6, 7] that the scalar particles are composite objects whose production rate may be larger than in the Standard Model. Recently it has been pointed out that hardly any experimental constraints exist on Higgs - gauge boson couplings. These could be affected by new physics at the scale of several TeV and the cross section for associated Higgs - photon production can even be orders of magnitude larger than the Standard Model Higgs expectation [8, 9] while the experimentally scrutinized Bjorken process could be reduced.

Based on about 3.5 million hadronic Z^0 decays, corresponding to 5 million produced Z^0's, we report on a search for a narrow resonance S^0 recoiling against a photon, where the S^0 decays into hadrons. In particular we search for decays where the S^0 is a scalar and, motivated by the expectation that the Higgs should couple to fermions f with strength proportional to their mass squared m_f^2, we study events with an isolated photon and bottom quarks. This analysis updates our previously published result that was based on a data sample that was more than two orders of magnitude smaller [10]. We also update our search for a resonance decaying into two photons produced in association with hadrons [11].

We start this paper by describing in Section 2 the selection of hadronic events with an isolated photon. In Section 3 we present the results of fits to the mass spectra of the hadronic system. We use three levels of cuts that progress from a more general search for a resonance to the specific signatures of a Higgs particle. In Section 4 the examination of hadronic events with two isolated photon candidates for a narrow resonance decaying into two photons is described. Conclusions are presented in Section 5.

2 The OPAL Detector and the Selection of Hadronic Z^0 Decays with an Isolated Photon

A detailed description of the OPAL detector can be found elsewhere [12]. Here we only review the central detector and the electromagnetic calorimeter, essential for this analysis. The central part consists of a system of cylindrical tracking detectors and is contained in a solenoidal magnetic field of 0.435 T. Close to the interaction point there is a two layer high precision silicon microvertex detector that is particularly suited to reconstruct secondary vertices. Three systems of drift chambers provide an accurate determination of the momenta of charged particles.

The detection efficiency for charged particles is close to 100% within the polar angle range $|\cos\theta| < 0.92$ where θ denotes the track angle with respect to the beam axis.

The barrel part of the electromagnetic calorimeter covers the entire azimuth and the polar angle range down to $|\cos\theta| < 0.82$. It consists of 9440 lead glass blocks, 24.6 radiation lengths deep, pointing towards the interaction region and each subtending an angular region of approximately 40×40 mrad^2. Each of the two endcap calorimeters consists of 1132 lead glass blocks parallel to the beam direction and covers the polar angle region of $0.81 \leq |\cos\theta| \leq 0.98$.

The analysis is based on an integrated luminosity of 140 pb^{-1}, collected with the OPAL detector at LEP between 1991 and 1994. The data were recorded at centre-of-mass energies between 88.28 GeV and 94.28 GeV around the Z^0 pole.

With the requirements described in reference [13] a sample of 3.509 million hadronic Z^0 decays has been selected. About 86% of these events were collected on the Z^0 pole. The silicon microvertex detector was operational for about 88% of the total sample. The acceptance of the hadronic events is estimated from Monte Carlo studies to be $\epsilon_{\rm had} = 0.984 \pm 0.004$ [13]. The background fraction from τ pairs and two photon processes was found to be less than 0.003.

From this sample, radiative Z^0 decays are selected by requiring an isolated photon candidate. To suppress hadronic backgrounds, mostly due to $\pi^0 \to \gamma\gamma$ that are in general of low energy and concentrated in the vicinity of jets, high energy isolated clusters in the electromagnetic calorimeter have been selected. A cluster from a photon candidate has to fulfill the following requirements (for details see reference [15]).

- It has to be within a fiducial volume $|\cos\theta| < 0.72$ or $0.82 < |\cos\theta| < 0.92$ of the lead glass calorimeter. The intermediate region $0.72 < |\cos\theta| < 0.82$ has not been used because the amount of material in front of the calorimeters increases up to a total of 8 radiation lengths leading to a substantial degradation of the energy resolution of the lead glass calorimeter.
- Its energy has to be larger than 5 GeV.
- No well measured track with a transverse momentum with respect to the beam of more than 250 MeV or any additional cluster in the lead glass calorimeter with an energy exceeding 250 MeV is allowed within an isolation cone of half-angle 10 degrees around the reconstructed flight direction of the photon candidate.
- To further suppress background from hadrons, the cluster properties are demanded to agree with those expected from a single photon. Due to the detector geometry these requirements are different for the barrel and endcap region.

  For the barrel region the requirements on the cluster properties are discussed in detail in reference [15]. To summarize, the number of blocks has to be smaller than 16, the energy weighted width of the cluster has to be smaller than 30 mrad and the photon hypothesis has to be supported by the value of a cluster shape variable that indicates the goodness of the fit to this hypothesis. These requirements result in a photon detection efficiency of (93.6 ± 1.6)%, measured with photons from the processes $e^+e^- \to \ell^+\ell^-\gamma$, $\gamma\gamma$, and $\gamma\gamma\gamma$, where $\ell^+\ell^-$ denotes either a muon or electron pair. No dependence of the efficiency on the photon energy has been observed for photon energies above 5 GeV.

In the endcap region ($0.82 \leq |\cos\theta| \leq 0.92$) the cluster width has to be smaller than 45 mrad and at least 70% of the cluster energy must be deposited in two blocks. The detection efficiency has been found to be (91.2±2.0)% for photons with energy between 5 and 30 GeV and ranges between 84% and 87% for photon energies above 30 GeV.

Additional losses are due to photon conversions in the central detector. The probability that a photon traversing the detector perpendicular to the beam direction converts to e^+e^- is $(6.3 \pm 1.2)\%$ [14].

After applying these cuts we are left with 25290 events containing isolated photon candidates. Standard Model contributions to this sample are due to hadrons decaying into photons ($\sim$ 11%), mainly from $\pi^0 \to \gamma\gamma$, photons emitted from the incoming electrons and positrons ($\sim$ 7%), and photons emitted from the outgoing quarks ($\sim$ 82%). To identify a potential Higgs particle we will search for a resonance structure in the hadronic mass spectrum. None of the background contributions leads to such a resonance behaviour at least for masses larger than $\sim$ 11 GeV, i.e. above the Υ region.

The dominant contribution is due to photon emission from quarks. As shown in several analyses [15, 16] QCD shower models and matrix element calculations give a good representation of the general properties of events with final state photons. Since the HERWIG model reproduces the overall photon yield well, we will compare our results with about 50 000 $q\bar{q}\gamma$ events generated with the HERWIG model [17] corresponding to 5.9 million hadronic Z^0 decays. To account for the better description of bottom production and decays by the JETSET model [18], we also use a sample of 20 000 $b\bar{b}\gamma$ events generated with this model. For the final comparison we combine the (u,d,s,c) events from HERWIG with the properly normalised b events from JETSET. Assuming four different Higgs masses samples each of 1000 generated $Z^0 \to H^0\gamma$ decays were used. To take into account detector effects, these events were subjected to a detailed simulation of the OPAL detector [19] and passed through the same reconstruction programs as the data.

3 Search for a Narrow Resonance

The search for a narrow resonance S^0 in the process $e^+e^- \to S^0\gamma$ at Z^0 energies proceeds in three steps addressing in turn more and more detailed properties expected for a Higgs particle. In all cases we search for a signal in the spectrum of the hadronic mass $M_{\rm had}$. We employ two methods of determining $M_{\rm had}$.

The first one uses the relation

$$M_{\rm had} \;=\; E_{\rm cm}\,\sqrt{1 - 2E_\gamma/E_{\rm cm}} \qquad (1)$$

that is based on the knowledge of the center of mass (c.m.) energy and of the photon energy alone. The energy resolution in the lead glass calorimeter is determined in two ways yielding consistent results. Firstly $e^+e^-\gamma$ and $\mu^+\mu^-\gamma$ events were used invoking massless three body kinematics and secondly Bhabha events were used by comparing well measured tracks and the energy observed in the calorimeter. For the latter Monte Carlo simulation was used to correct

for effects from bremsstrahlung of the electrons in the material of the detector and it was shown that the resolution for photons and electrons agree for the energy range of importance for this analysis. In the absence of initial state photon emission the hadronic mass resolution σ_M decreases from about 5.8 GeV at $M_{\mathrm{S}^0} = 20$ GeV to about 0.6 GeV at $M_{\mathrm{S}^0} = 80$ GeV. Initial state radiation leads to a tail of apparent higher masses, but its effect at the Z^0 peak is small.

The second method leads to better resolutions at low hadronic masses and uses three body kinematics based on properties of the hadronic system. In a first step the hadrons are combined into exactly two jets applying the JADE-E0 jet finding algorithm [20] to all tracks and non-associated clusters in the calorimeter. The photon candidate is excluded from the jet definition. Making use of the relatively good knowledge of the jet direction of $\sim$75 mrad, the energy of jet i is then obtained from:

$$E_i \;=\; E_{cm}\frac{\beta_\gamma\beta_j \sin\alpha_{j\gamma}}{\sum_{l,m}\beta_l\beta_m \sin\alpha_{lm}} \tag{2}$$

where j denotes the other hadron jet, and α_{lm} is the angle between jets or photon l and m. The sum in the denominator runs over the three possibilities of combining the two hadronic jets and the photon. The velocity

$$\beta_k \;=\; \frac{|\sum \vec{p_i}|}{\sum E_i}, \tag{3}$$

is obtained by summing over the measured momenta and energies of charged tracks and clusters in the electromagnetic calorimeter assigned to jet k. The velocity of the photon is β_γ=1. The mass of the hadronic system is finally determined from

$$M^2_{\mathrm{had}} \;=\; (E_1+E_2)^2 - (\beta_1 E_1)^2 - (\beta_2 E_2)^2 - 2\beta_1\beta_2 E_1 E_2 \cos\alpha_{12} \tag{4}$$

From simulation studies we find the mass resolution using this method to be independent of mass. For large values of M_{had} the σ_M of the second method is significantly worse than for the first method. We therefore measure the precision of the second method by comparing the masses obtained from the two methods for $M_{\mathrm{had}} > 60$ GeV. We find $\sigma_M = 3.1\pm0.1$ GeV for the second method. Since the methods are independent, we finally use the weighted average of the result of the two methods.

The hadronic mass spectrum is analysed in the following stages with increasingly stringent cuts:

1. No additional requirement is imposed. This provides a very general search for a resonance signal (Sect.3.1).
2. A cut on the angle of the quark with respect to the flight direction of the hadronic system is applied, enriching a potential scalar resonance contribution (Sect.3.2).
3. Additional algorithms enhancing the fraction of bottom quarks are invoked to gain sensitivity to the channel $\mathrm{S}^0 \to \mathrm{b\bar{b}}$ (Sect.3.3).

In each case we fit a generalized likelihood function to the mass spectrum between 15 and 83 GeV, assuming some resonance mass M_{res}

$$\mathcal{L} \;=\; e^{-\nu}\prod_{i=1}^{N}(B + \frac{N_{\mathrm{res}}}{\sqrt{2\pi}\sigma_M}\exp[-\frac{(M_i - M_{\mathrm{res}})^2}{2\sigma_M^2}]) \;=\; e^{-\nu}\prod_{i=1}^{N}F(M_i), \tag{5}$$

where N is the number of observed events,

$$\nu = \int_{M=15\,GeV}^{M=83\,GeV} F(M)dM \tag{6}$$

the number expected from the fit, and σ_M is the weighted average resolution from the two methods discussed above. The free parameter $N_{\rm res}$, constrained to be greater than or equal to 0, accounts for the potential resonance production. Several phenomenological parametrisations of the background were studied. We adopt the functional form

$$B \;=\; x_1 \cdot (1 \;+\; x_2 M_i \;+\; x_3 \exp[x_4 M_i^{x_5}]) \tag{7}$$

as the default parametrisation of the background. Here the five x_i are free parameters. Interpreting the results in terms of χ^2, we find typical values of 120 for 130 degrees of freedeom, slightly depending on the assumed resonance mass and the selection. To study potential systematic uncertainties we repeat the fit in the restricted mass range $\pm 6\sigma_M$ around the assumed resonance mass. In general, this gives similar branching ratio limits to those from the fit over the full mass range. Details will be given in the following sections. Other parametrisations that were tried, such as fixing the exponent $x_5 = x_4 = 1$ generally gave worse fit qualities. We vary $M_{\rm res}$ in steps of 500 MeV for values of $20.25 \leq M_{\rm res} \leq 79.75$ GeV, i.e. at each stage we consider 120 possible resonance masses. The limits on the mass interval are chosen to avoid the potential Υ contribution at low $M_{\rm res}$ and the rapidly falling acceptance close to $E_{\rm cm} - 5$ GeV. For the presentation of background curves in the figures, we take at each mass value the background level obtained from the fit with $M_{\rm res}$ fixed at that point.

From the background given by the fit we derive a 95% confidence level (C.L.) upper limit for the product branching ratio of the $\rm Z^0$ into some resonance $\rm S^0$ of mass $M_{\rm res}$:

$$BR(\rm Z^0 \to S^0\gamma) \cdot BR(\rm S^0 \to q\bar{q}) \;<\; \frac{1}{\epsilon_{\rm acc}} \frac{\rm N_{95\%}}{\rm N_{had}} \rm BR(Z^0 \to had)\epsilon_{had}. \tag{8}$$

Here $N_{95\%}$ is the maximum number of signal events that can be excluded from the fit with 95% confidence. It is calculated from the number of background and observed events according to the procedure suggested in [21]. The background yield is obtained by integrating the fit result within $\pm 2\sigma_M$ around the resonance mass. The number of signal events is taken as the difference between observed and background yield in this mass range but has to be at least zero. The acceptance of the selected type of events is denoted by $\epsilon_{\rm acc}$ and is the product of efficiencies due to various sources discussed below. $N_{\rm had}$ is the background corrected observed number of hadronic events considered in this analysis (cp. Section 2), $BR(\rm Z^0 \to \mathit{had}) = 0.695 \pm 0.003$ is the measured hadronic $\rm Z^0$ branching ratio [13] and $\epsilon_{\rm had}$ the acceptance of hadronic events. The efficiencies of observing events with a potential scalar particle are calculated using a simulation of $\rm Z^0 \to S^0\gamma$ including initial state radiation [22] and quark fragmentation as implemented in JETSET [18] with parameters optimised to describe inclusive hadronic $\rm Z^0$ decays [23], followed by the simulation of the detector response as discussed above. The selections used for the first two stages of the analysis were found to be independent of the quark flavour of the $\rm S^0$ decay and therefore the corresponding efficiencies were determined from a mixture of all flavours. Systematic errors of these efficiencies are taken into account in deriving upper limits for the production cross section. We conservatively reduce all efficiencies by one standard deviation. Two contributions were considered as overall efficiencies:

- Because signal and background were integrated over a region of width $\pm 2\sigma$, the efficiency due to the resonance shape is $\epsilon_{\rm res} = 0.95 \pm 0.02$. Distortions due to initial state radiation are taken into account and the uncertainty allows for a 10% variation of σ_M.

- The photon detection efficiency accounts for losses due to conversions and cuts on the cluster properties and is found to be $\epsilon_{\gamma-\rm eff} = 0.860 \pm 0.025$. Here the dependence on the polar angle of the photon conversion probability, on the photon energy, and on the cluster quality (described in section 2) is taken into account.

We interpret our results as they apply to theoretical expectations. The partial decay rate as expected in the Standard Model and its extensions can be expressed as

$$\Gamma(\mathrm{Z}^0 \to \gamma \mathrm{S}^0) \;=\; \frac{1}{6}\alpha M_{\mathrm{Z}^0}\left(1 - \frac{M_{\mathrm{S}}^2}{M_{\mathrm{Z}^0}^2}\right)^3 C_{\rm eff}, \tag{9}$$

where $C_{\rm eff}$ is the model specific coupling and $\alpha \sim 1/128$ the electromagnetic coupling at the Z^0 mass. In the Standard Model the dominant contribution is due to a W loop yielding [4]

$$C_{\rm eff}^{SM} \;=\; \frac{\alpha^2}{64\pi^2}\frac{1}{\sin^4\theta_w \cos^2\theta_w}(4.55 + 0.31\frac{m_S^2}{m_W^2})^2, \tag{10}$$

or $C_{\rm eff}^{SM} \sim 5\times 10^{-5}$. Here θ_w is the weak mixing angle and m_W the W -boson mass. As described below, we do not have sufficient sensitivity to the Standard Model Higgs boson, whereas other models of the production of some scalar particle are significantly constrained. A model for the production of a composite Higgs boson [6] gives

$$C_{\rm eff}^{comp} = (\kappa_1^2 + \kappa_2^2)\frac{M_{\mathrm{Z}^0}^2}{\Lambda_{comp}^2}, \tag{11}$$

where κ_i are some unknown couplings and Λ_{comp} the compositeness scale. In models with anomalous $Z^0 S^0 \gamma$ or $\gamma S^0 \gamma$ couplings

$$C_{\rm eff}^{anom} = \cos\theta_w^2 (\sum_i d_i)^2, \tag{12}$$

where d_i are either CP conserving or violating couplings related to some scale of new physics [9].

We take into account variations of the production yield due to the different c.m. energies used for this search. Even for high masses the change compared to using the formulae at the Z^0 pole is marginal. Since, in principle, a resonance could be produced without the intermediate production of a Z^0 we also interpret our result in terms of the production cross section

$$\sigma(\mathrm{e^+e^-} \to \mathrm{S}^0\gamma) \;<\; \frac{1}{\epsilon_{\rm acc}}\frac{\mathrm{N}_{95\%}}{\int \mathrm{L}\,\mathrm{dt}}, \tag{13}$$

where $\int \mathrm{L}\,\mathrm{dt}$ is the integrated luminosity of 140 pb^{-1}.

3.1 Inclusive Mass Spectrum

We discuss as a first step the search before imposing further cuts. We show the measured spectrum of 14658 events with M_{had} between 15 and 83 GeV in Figs.1a,b. No obvious resonance structure is observed. We also display the normalised distribution of the mass spectrum for final state photons as expected by the HERWIG and JETSET models. The agreement is reasonable. We fit the distribution to equation (5) and obtain the background yield indicated by the line in Figs.1a,b. The difference between data and background fit is shown in Fig.1c.

We translate this measurement into a 95% CL upper limit according to the procedure discussed previously. The efficiency for retaining a resonance decay depends on the angular distribution of the quarks with respect to the S^0 flight direction. We assume an isotropic decay of the S^0. The total efficiency is given by

$$\epsilon_{\rm acc} \;=\; \epsilon_{\rm res} \times \epsilon_{\gamma-{\rm eff}} \times \epsilon_{\rm geom} \tag{14}$$

where $\epsilon_{\rm geom}$ takes into account the additional losses due to the restricted polar angle and to the isolation cone. Mainly due to the requirement on the photon isolation the efficiency decreases slightly with increasing $M_{\rm res}$ which we parametrise as ($M_{\rm res}$ in GeV)

$$\epsilon_{\rm geom} \;=\; 0.72 \;+\; 0.0015(60 - M_{\rm res}). \tag{15}$$

We assign an error of 0.03 to account for uncertainties due to fragmentation effects that could affect the isolation requirement (cp. discussion in [15]).

Fitting the function of equation (5) to the observed spectrum yields 95% CL upper limits on the product branching ratio $BR(Z^0 \to S^0\gamma)BR(S^0 \to q\bar{q})$, as shown in Fig.1d. The limits vary between approximately 10^{-5} and $4{\cdot}10^{-5}$. These branching ratios correspond to production cross sections between 0.4 and 2 pb. Restricting the fit range to a mass window of $\pm 6\sigma_M$ leads mostly to identical limits. For masses below 60 GeV the limits obtained are about a factor 5 – 100 above the Standard Model expectation. However, in this range, Higgs production with an effective coupling larger than $\sim 5 \times 10^{-3}$ is excluded. For very high masses these results are less restrictive. Amongst the 120 bins in this distribution the largest excess is observed at $M_{\rm res}$=38.75 GeV, where the background fit yields 670.9 events, but 784 are observed. This corresponds to a 4.2 standard deviation upward fluctuation of the background in this particular bin, taking statistical errors only into account. A possible source of systematic uncertainty could result from the choice of different background parametrizations. To study this, we performed the fit with a restricted mass window, or including a quadratic term $x_6 M_i^2$ in equation (7) and found the number of background events decreased, while the fit quality was essentially unchanged.

3.2 Cutting on the Decay Angle

We increase the sensitivity to a resonance of spin 0 by making use of its expected isotropic decay distribution. We determine the angle of the two quarks in the hadronic rest system with respect to the S^0 flight direction. To this end we boost all hadrons into their common rest

system using the four-momentum of the photon:

$$E_{had} = \sqrt{M_{\rm had}^2 + p_\gamma^2}, \qquad \vec{\beta}_{\rm had} = -\vec{p}_\gamma / E_{had} \qquad \gamma_{\rm had} = \frac{E_{\rm had}}{M_{\rm had}}. \tag{16}$$

In this rest system we then determine the thrust direction and calculate its angle θ^* to the photon. Whereas photons from quark bremsstrahlung and hadronic background tend to have small angles with respect to the thrust direction, those from $Z^0 \to S^0\gamma$ decay would be isotropically distributed. We require $|\cos\theta^*| < 0.7$, which additionally rejects about 60% of the background while retaining between 60% (for $M_{\rm res} = 20$ GeV) and 78% (for $M_{\rm res} = 80$ GeV) of the signal events. We use the parametrisation ($M_{\rm res}$ in GeV)

$$\epsilon_{\theta^*} = 0.725 - 0.003(60 - M_{\rm res}) \tag{17}$$

as an additional factor multiplying $\epsilon_{\rm acc}$. We assign an error of 0.025 to this efficiency to take into account the statistical uncertainty of the simulation and potential misrepresentations in the simulation of the reconstruction of the quark direction. As discussed in [24] this uncertainty is less than one degree. One should note that the region of $|\cos\theta^*| > 0.7$ is already depleted by the isolation requirement on the photon, especially for high masses $M_{\rm had}$. For a scalar particle the *combined* efficiency $\epsilon_{\rm geom} \cdot \epsilon_{\theta^*}$ is about 0.50, with only a small dependence on the resonance mass.

After the $\cos\theta^*$ requirement 5701 events are retained for $M_{\rm had}$ between 15 and 83 GeV. The resulting spectrum is shown in figs.2a,b. The fit to this distribution according to equation (5) is indicated by the full line. No significant resonance structure is observed which can also be seen from fig. 2c showing the difference of data and background fit. Also shown is the result of the combined HERWIG and JETSET simulation of final state photon emission normalised to the observed number of events. It is in reasonable agreement with the data.

Taking the efficiencies into account, we translate the results of a fit of equation (5) into the 95% CL upper limits on $B(Z^0 \to S^0\gamma) \cdot BR(S^0 \to q\bar{q})$ shown in figure 2d. Compared to the overall sample discussed in the previous section, the sensitivity is typically improved by 25% yielding an upper limit of $\mathcal{O}(1 - 4 \cdot 10^{-5})$ or a production cross section of ~ 0.6 pb. The cross check with a fit in a limited mass range yields identical results for most of the mass range but somewhat worse limits are obtained when the default fit prefers some resonance contribution. These results correspond to limits on the production of a scalar resonance with effective couplings larger than $C_{\rm eff} \sim 2 \times 10^{-4}$ at 20 GeV and $C_{\rm eff} \sim 5 \times 10^{-2}$ at 80 GeV. Amongst the 120 bins in this distribution the largest excess over the fitted background is observed at $M_{\rm res}$=67.25 GeV, where 484 events are observed for a background of 426.3. This corresponds to a 2.8 standard deviation upward fluctuation of the background.

3.3 Selecting bottom decays of S^0

In a final step we search for the specific decay $S^0 \to b\bar{b}$ by tagging b quark events using their secondary vertices and their decay into energetic electrons and muons. Bottom tagging is expected to lead to a substantial reduction of the Standard Model background since only ~9% of final state photons are expected to originate from bottom quarks. On the other hand, for a

Standard Model Higgs, the decay branching ratio $BR(S^0 \to b\bar{b})$ is about 90%. Within extensions of the Standard Model this branching ratio may change. For example, in Supersymmetric models it may be reduced according to the ratio of the two vacuum expectation values and the mixing angle between the two neutral scalars. Within composite scenarios the branching ratio may be reduced or increased depending on the model. Therefore, depending on its actual branching ratio into bottom pairs, events of the type $b\bar{b}\gamma$ may be more sensitive to a scalar resonance.

Secondary vertex finding was carried out separately for each reconstructed jet in an event. Jets are defined by the E0-JADE iterative clustering algorithm [20] requiring that the maximum mass squared $2E_iE_j(1-\cos\alpha_{ij})$ of two particles or precombined particles within a jet does not exceed $(7\ \mathrm{GeV})^2$. Here the E_i are the energies and α_{ij} the opening angle of the pair of particles. To reconstruct a secondary vertex we adopt the algorithm described in ref.[25]. For each reconstructed secondary vertex, the vertex decay length L was defined as the distance of the secondary vertex from the primary vertex, projected onto a direction given by the total momentum vector (in the plane transverse to the beam direction) of the tracks assigned to the secondary vertex. The total vertex momentum vector was also used to determine the sign of the decay length: $L>0$ if the secondary vertex was displaced from the primary vertex in the same direction as the total momentum, and $L<0$ otherwise. To each of the jets we assign a decay length significance, defined as the maximum signed decay length L divided by its error σ_L.

For the lepton tag we use the procedure discussed in [25] to identify muons and electrons.

We finally retain an event if it has

- a secondary vertex with three assigned tracks and $L/\sigma_L > 6$, or
- a secondary vertex with at least four assigned tracks and $L/\sigma_L > 4$, or
- an electron candidate with momentum larger than 2 GeV and a transverse momentum with respect to the associated jet axis of at least 1.1 GeV, or
- a muon candidate with momentum larger than 3 GeV and a transverse momentum with respect to the associated jet axis of at least 1.2 GeV.

For the part of the data where the silicon microvertex detector was operational, we find that for the selected events with $|\cos\theta^*|$ <0.7, the tagging efficiency for $S^0 \to b\bar{b}$ is independent for $M_{\mathrm{res}} < 60$ GeV and increases as

$$\epsilon_{\mathrm{b}} \;=\; 0.50 \;-\; 0.006(60 - M_{\mathrm{res}}) \tag{18}$$

for $M_{\mathrm{res}} \geq 60$ GeV. Here M_{res} is taken in GeV. To account for uncertainties in the bottom lifetimes and the simulation of the detector we assign a systematic error of 0.025 to ϵ_{b}. This is estimated from comparing the efficiency of double tagged events in the data and in the simulation in inclusive Z^0 decays and takes into account the limited statistics of the simulation. As mentioned in Section 2, the microvertex detector was not used for about 12% of the data. From simulation studies the efficiency of tagging these events is found to be a factor two lower. We therefore scale ϵ_{b} by 0.94.

As expected, the final state photon background is significantly reduced after this cut. According to the simulation only about 7% of the final state photons from light and charm quarks are retained giving a bottom fraction in the final state sample of about 40%. The spectrum of the decay length significance is shown in Fig.3a together with the normalised expectation of the simulation. Also shown is the expected distribution from bottom quarks indicating their enrichment for large decay length significances. The agreement is reasonable. In particular no discrepancy between data and simulation is observed for large values of the decay length significance which could indicate a deviation in the predicted bottom contribution.

Only 488 events are retained in the mass range $20 < M_{\rm res} < 80$ GeV, which compares well with the number of 513$\pm$16 expected by the QCD models for final state photon radiation, after normalising to the event yield without bottom tagging. Out of these 488 events, 477 events are accepted by the lifetime tag, and 21 events by the lepton tag. The mass spectrum is shown in Figs.3b,c. No significant resonance structure is observed which is underlined by Fig.3d showing the difference between data and the background fit. Also the shape of the expectation agrees well with the data, suggesting that they can be explained by final state photon emission alone.

We fit the function of equation (5) to this spectrum and obtain the 95% CL upper limit of the product branching ratio $BR(\mathrm{Z}^0 \to \mathrm{S}^0\gamma) \cdot BR(\mathrm{S}^0 \to \mathrm{b\bar{b}})$. The fitted background distribution is shown in Figs.3b,c. The corresponding limits are displayed in Fig.3e. Also shown is the expectation for the Standard Model and for various values of the effective coupling $C_{\rm eff}$ assuming a branching ratio $BR(\mathrm{S}^0 \to \mathrm{b\bar{b}})$ of 100%.

Assuming a significant branching ratio of the S^0 into bottom quarks, the bottom tagging requirement provides a gain of about factor of two compared to the sensitivity with no tagging. This sets limits on $BR(\mathrm{Z}^0 \to \mathrm{S}^0\gamma) \cdot BR(\mathrm{S}^0 \to \mathrm{b\bar{b}})$ of typically between 0.7 and 2 $\cdot 10^{-5}$ or a production cross section between 0.3 and 0.8 pb. Restricting the fit to a mass window around the resonance mass yields in general $\sim$ 10% worse limits for $M_{res} < 40$ GeV and better limits for larger masses. In this case the fit with $x_4 = x_5 = 1$ also gives fits of acceptable quality and can be used as a systematic check. Its results are very close to the other two fits. Amongst the 120 bins in this distribution, the largest excess is at $M_{\rm res} = 62.75$ GeV, where we observe 56 events and the background fit yields 40.9 events. This corresponds to a 2.4 standard deviation upward fluctuation. In terms of extensions of the Standard Model, we can exclude the production of a scalar resonance with $C_{\rm eff} > 3 \times 10^{-4}$ for masses below 35 GeV, and $C_{\rm eff} > 10^{-4}$ for masses below 60 GeV. For $M_{\rm res}$=80 GeV the limit corresponds to $C_{\rm eff} \sim 5 \times 10^{-3}$.

4 Search for a Resonance Decay into Two Photons

We extend this analysis to a search for a potential two photon decay mode of a resonance. Such a process has aroused increased interest after the observation of four events of the type $(\mathrm{e^+e^-})$, $(\mu^+\mu^-)$ and $\gamma\gamma$ where the two photon invariant mass was around 60 GeV [26]. As discussed in [8], extremely favourable anomalous couplings could lead to a decay rate of $S^0 \to \gamma\gamma$ that is substantially larger than the Standard Model one. Here we study the invariant mass spectrum of two photons produced in association with quarks. Previous studies of this topology have not found any evidence for a resonance production [11, 27].

Starting from the sample described in Section 2, we require a second photon candidate imposing identical requirements as for the first photon, i.e. on its energy ($E_\gamma > 5$ GeV), isolation (no additional energy within 10 degrees), and its cluster properties. Note that in contrast to our previous publication we also impose cluster shape requirements for photon candidates in the endcap region. We find 144 events in agreement with 131$\pm$15 events predicted by the HERWIG simulation. The typical mass resolution for two photon masses above 40 GeV is about 2 GeV.

The two photon mass spectrum is shown in fig. 4. No significant mass structure is observed. We observe three events with a mass of more than 40 GeV where HERWIG predicts 5.4 $\pm$ 3.0. The highest two photon mass is at 77 GeV. As already shown in [11], one event is observed with a mass around 60 GeV.

To estimate the efficiency for finding a two photon resonance, we generated events of the type $Z^0 \to Z^{*0}S^0$, where the off-shell Z^{*0} decays into quarks and the scalar S^0 into two photons. For S^0 masses between 30 and 70 GeV we observe an efficiency of 44$\pm$3% which is independent of the two photon mass. Based on this efficiency and conservatively neglecting background contributions, we can set the following upper 95% confidence limit on the product branching ratio for masses of larger than 40 GeV:

$$BR(Z^0 \to S^0 q\bar{q}) \cdot BR(S^0 \to \gamma\gamma) \;<\; 2 \times 10^{-6}. \tag{19}$$

At lower masses the result is less restrictive.

5 Conclusion

Previous publications [10, 28] on a narrow resonance decaying into quarks produced in association with a photon were based on up to 0.5 million produced Z^0 events and set limits of $\mathcal{O}(4$ pb) on the production cross section for some resonance S^0. This analysis is based on approximately 5 million produced Z^0 events. We find no evidence for a resonance and place upper limits with 95% confidence level on the production cross section of typically 0.8 pb for a scalar resonance decaying into hadrons. Following theoretical expectations that such a resonance should decay mostly into bottom quarks allows us to exclude a production cross section of typically 0.5 pb. Interpreting these results in terms of Z^0 branching ratios leads to typical results of

$$BR(Z^0 \to S^0\gamma) \cdot BR(S^0 \to q\bar{q}) \;<\; 2 \times 10^{-5} \tag{20}$$

or

$$BR(Z^0 \to S^0\gamma) \cdot BR(S^0 \to b\bar{b}) \;<\; 1 \times 10^{-5}. \tag{21}$$

These limits are considerably more stringent than previously obtained. They can be used to exclude non-standard Higgs production as considered in several models. Expressing the limits in terms of the effective coupling C_{eff}, we can exclude Higgs production with $C_{\text{eff}} > \mathcal{O}(10^{-3} - 10^{-4})$ at least for masses below 60 GeV.

We also update our search for a narrow resonance decaying into two photons which is produced in association with two quarks. No resonance structure is observed and for resonance masses between 40 and 80 GeV we find

$$BR(Z^0 \to S^0 q\bar{q})\mathrm{BR}(S^0 \to \gamma\gamma) \;<\; 2 \times 10^{-6}. \tag{22}$$

at 95% confidence.

6 Acknowledgements

Discussions and valuable comments from F.Boudjema, G.Gounaris, M.Spira, and P.Zerwas are gratefully acknowledged.
It is a pleasure to thank the SL Division for the efficient operation of the LEP accelerator, the precise information on the absolute energy, and their continuing close cooperation with our experimental group. In addition to the support staff at our own institutions we are pleased to acknowledge the
Department of Energy, USA,
National Science Foundation, USA,
Particle Physics and Astronomy Research Council, UK,
Natural Sciences and Engineering Research Council, Canada,
Israel Ministry of Science,
Israel Science Foundation, administered by the Israel Academy of Science and Humanities,
Minerva Gesellschaft,
Japanese Ministry of Education, Science and Culture (the Monbusho) and a grant under the Monbusho International Science Research Program,
German Israeli Bi-national Science Foundation (GIF),
Direction des Sciences de la Matière du Commissariat à l'Energie Atomique, France,
Bundesministerium für Forschung und Technologie, Germany,
National Research Council of Canada,
Hungarian Foundation for Scientific Research, OTKA T-016660, and OTKA F-015089.

References

[1] P. Higgs, Phys. Lett. 12 (1964) 132;
R. Brout and F. Englert, Phys. Rev. Lett. 13 (1964) 321.

[2] J. D. Bjorken, in Proceedings of the 1976 Summer Institute on Particle Physics Stanford, edited by M. C. Zipf (SLAC, Stanford, CA, 1977) p.1.

[3] ALEPH Collaboration, D. Buskulic et al., Phys. Lett. B313 (1993) 299;
DELPHI Collaboration, P. Abreu et al., Nucl. Phys. B421 (1994) 385;
L3 Collaboration, O. Adriani et al., Phys. Lett. B303 (1993) 391;
OPAL Collaboration, R. Akers et al., Phys. Lett. B327 (1994) 397.
Results are combined e.g. by F. Richard in Proceedings of the XXVII International Conference on the High Energy Physics, 20-27 July 1994, Glasgow, Scotland, UK ed. P.J. Bussey and I.G. Knowles.

[4] R.N. Cahn, M.S. Chanowitz and N. Fleishon, Phys. Lett. B82 (1979) 112;
L.Bergström and G.Hulth, Nucl.Phys. B259 (1986) 137, erratum ibid B276 (1986) 744;
A.Barroso, J.Pulido and J.C.Romao, Nucl.Phys. B267 (1986) 509;
a recent calculation can be found in A.Abbasabadi et al., Phys. Rev. D52 (1995) 3919.

[5] G. Gamberini, G.F. Giudice, and G. Ridolfi, Nucl. Phys. B292 (1987) 237.

[6] D. Düsedau and J. Wudka, Phys. Lett. B180 (1986) 290.

[7] F.Renard, Phys. Lett. B126 (1983) 59, Phys. Lett. B132 (1983) 449;
L. Randall and N. Rius, Phys. Lett. B309 (1993) 365.

[8] K. Hagiwara and M.L. Strong, Z. Phys. C62 (1994) 99;
K. Hagiwara, R. Szalapski, and D. Zeppenfeld, Phys. Lett. B318 (1993) 155.

[9] G.J. Gounaris, J. Layssac and F. Renard, Z. Phys. C65 (1995) 245;
J.M. Hernandez, M.A. Perez, and J.J. Toscano, Phys. Rev. D51 (1995) R2044;
G.J.Gounaris, F.M.Renard and N.D.Vlachos, preprint PM-95-30, THEP-TP-95-08.

[10] OPAL Collaboration, M.Z. Akrawy et al., Phys. Lett. B246 (1990) 285.

[11] OPAL Collaboration, P. Acton et al., Phys. Lett. B311 (1993) 391.

[12] OPAL Collaboration, K. Ahmet et al., Nucl. Instr. Meth. A305 (1991) 275;
OPAL Collaboration, P.Allport et al., Nucl.Instrum. and Meth. A324 (1993) 34;
OPAL Collaboration, P.Allport et al., Nucl.Instrum. and Meth. A346 (1994) 476.

[13] OPAL Collaboration, G. Alexander et al., Z. Phys. C52 (1991) 175.

[14] OPAL Collaboration, P. D. Acton, Z.Phys. C58 (1993) 405.

[15] OPAL Collaboration, G. Alexander et al, Phys. Lett. B264 (1991) 219;
OPAL Collaboration, P. D. Acton, Z.Phys. C54 (1992) 193.

[16] L3 Collaboration, O. Adriani et al., Phys. Lett. B292 (1992) 472;
ALEPH Collaboration, D. Buskulic et al., Z. Phys. C57 (1993) 17.

[17] G. Marchesini et al., Comp. Phys. Comm. 76 (1992) 464.

[18] T. Sjöstrand, Comp. Phys. Comm. 39 (1986), 347; JETSET, Version 7.r4

[19] R. Brun et al., GEANT3 User's Guide, CERN DD/EE/84-1 (1989);
J. Allison et al., Nucl. Instr. Meth. A317 (1992) 47.

[20] JADE Collaboration, W. Bartel et al., Z. Phys. C33 (1986) 23;
JADE Collaboration, S. Bethke et al., Phys. Lett. B123 (1988) 235.

[21] Particle Data Group, Phys. Rev. D50 (1994) 1173.

[22] F. A. Berends, R. Kleiss and S. Jadach, Nucl. Phys. B202 (1982) 63.

[23] OPAL Collaboration, P.D.Acton et al., Z. Phys. C58 (1993) 357.

[24] OPAL Collaboration, P. D. Acton et al., Z. Phys. C54 (1992) 193.

[25] OPAL Collaboration, R. Akers et al., Z. Phys. C65 (1995) 17.

[26] L3 Collaboration, O. Adriani et al., Phys. Lett. B295 (1992) 337.

[27] ALEPH Collaboration, D. Buskulic et al., Phys. Lett. B308 (1993) 425;
L3 Collaboration, O. Adriani et al., Phys. Rep. 236 (1993) 1.

[28] ALEPH Collaboration, D. Decamp et al., Phys. Rep. 216 (1992) 253;
DELPHI Collaboration, P. Abreu et al., Z. Phys. C53 (1992) 555;
L3 Collaboration, O. Adriani et al., Phys. Rep. 236 (1993) 1.

Figure Captions

Fig. 1 (a) Spectrum of the hadronic mass of Z^0 decays with an isolated photon candidate in bins of 1 GeV. Also shown is the normalised expectation of the QCD shower model for the spectrum in events with photon emission from quarks (histogram) and the fitted background distribution (line). (b) The high mass part of the spectrum for data and fitted background in bins of 500 MeV. (c) Difference between observed number of events and fitted background for resonance masses considered per 1 GeV bin. (d) 95% confidence upper limit for the production of a narrow resonance decaying into hadrons as a function of its mass. Also shown are the expectations for a Standard Model Higgs and production of a scalar particle in composite models, assuming various compositeness scales.

Fig. 2 (a) Spectrum of the hadronic mass in bins of 1 GeV of Z^0 decays with an isolated photon candidate after a cut in the angle between jet and photon. Also shown is the corresponding normalised expectation of the QCD shower model for the spectrum in events with photon emission from quarks (histogram) and the fitted background distribution (line). (b) The high mass part of the spectrum for data and fitted background in bins of 500 MeV. (c) Difference between observed number of events and fitted background for resonance masses considered per 1 GeV bin. (d) 95% confidence upper limit for the production of a narrow scalar resonance decaying into hadrons as a function of its mass. Also shown are the expectations for a Standard Model Higgs and a production of a scalar particle in composite models, assuming various compositeness scales.

Fig. 3 (a) Spectrum of the decay length significance after a cut in the angle between jet and photon and requiring a secondary vertex in the event with at least three assigned tracks. The data (error bars) are compared to the spectrum for events with final state photons as expected by the QCD shower model (histogram). The hashed area shows the model expectation for events with photon emission from bottom quarks. (b) Spectrum of the hadronic mass in bins of 1 GeV of Z^0 decays with an isolated photon candidate after a cut in the angle between jet and photon and tagging for bottom production. Also shown is the corresponding expectation of the QCD shower model for the spectrum in events with photon emission from quarks (histogram). The number of events is normalised to the number expected without the bottom tagging requirement. The line denotes the fitted background distribution. (c) The high mass part of the spectrum for data and fitted background in bins of 500 MeV. (d) Difference between observed number of events and fitted background for resonance masses considered per 1 GeV bin. (e) 95% confidence upper limit for the partial decay width of a Z^0 into a narrow scalar resonance decaying into quarks times its branching ratio into bottom quarks as a function of its mass. Also shown are the expectations for a Standard Model Higgs and a production of a scalar particle in composite models, assuming various compositeness scales. In both cases the branching ratio $BR(S^0 \to b\bar{b})$ was assumed to be 100%.

Fig. 4 Spectrum of the invariant mass of two isolated photons in the process $e^+e^- \to \gamma\gamma$ + hadrons at Z^0 energies.

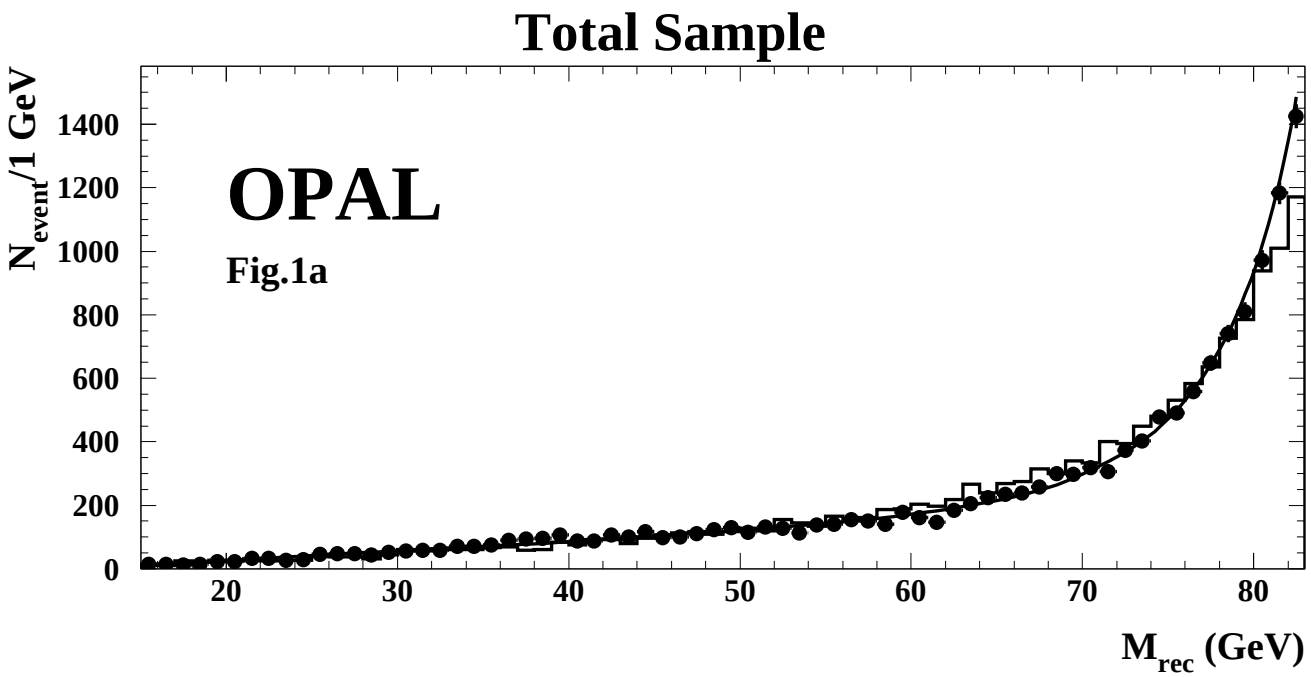
Total Sample
OPAL
Fig.1a
N_event/1 GeV
M_rec (GeV)

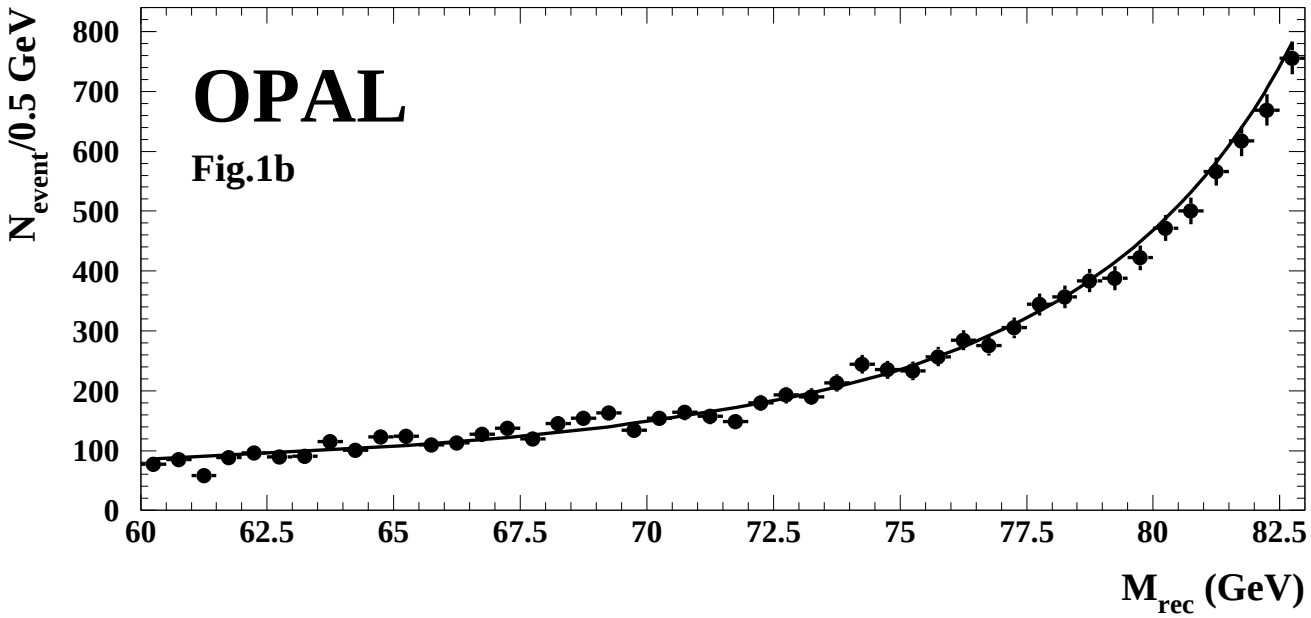
OPAL
Fig.1b
N_event/0.5 GeV
M_rec (GeV)

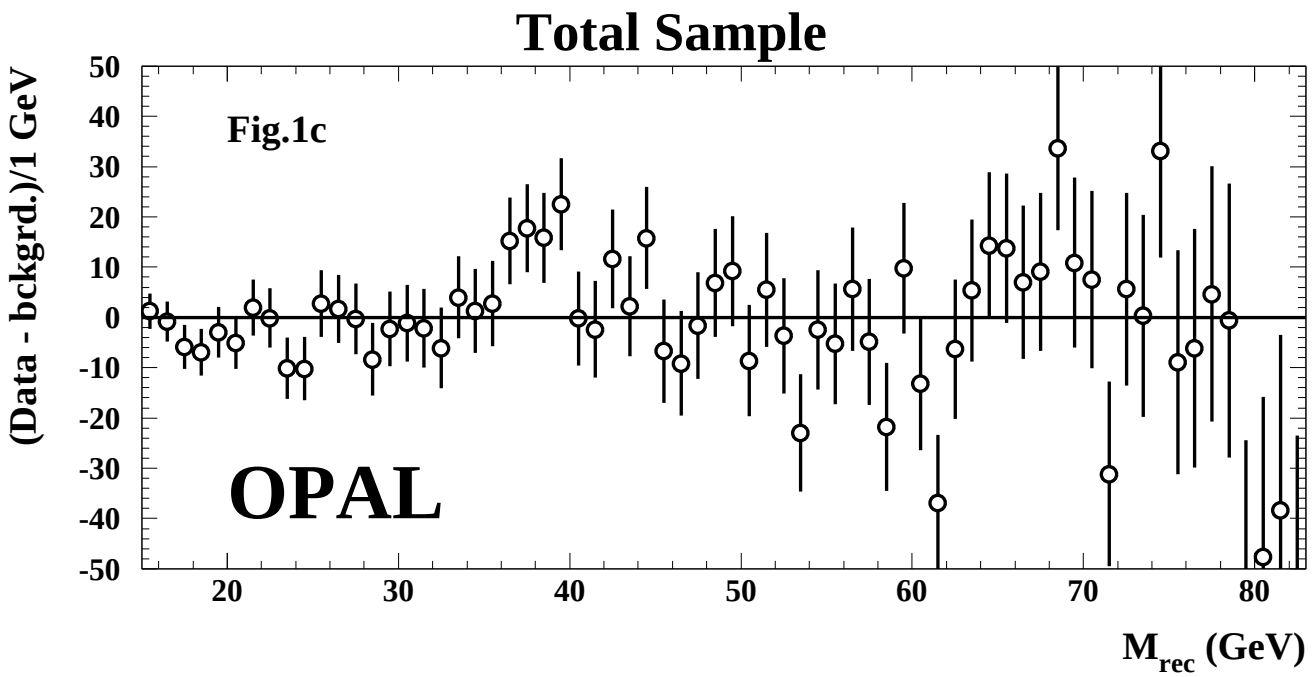
Total Sample
Fig.1c
OPAL
(Data - bckgrd.)/1 GeV
M_rec (GeV)

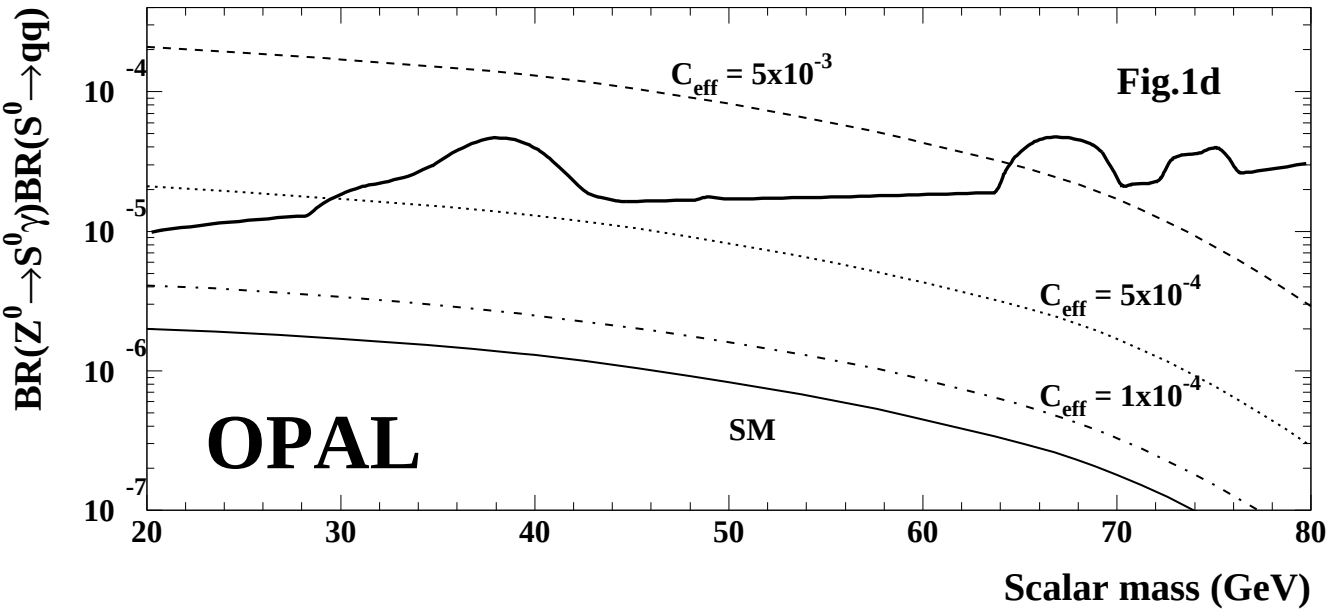
Fig.1d
C_eff = 5x10^-3
C_eff = 5x10^-4
C_eff = 1x10^-4
SM
OPAL
BR(Z^0→S^0γ)BR(S^0→qq)
Scalar mass (GeV)

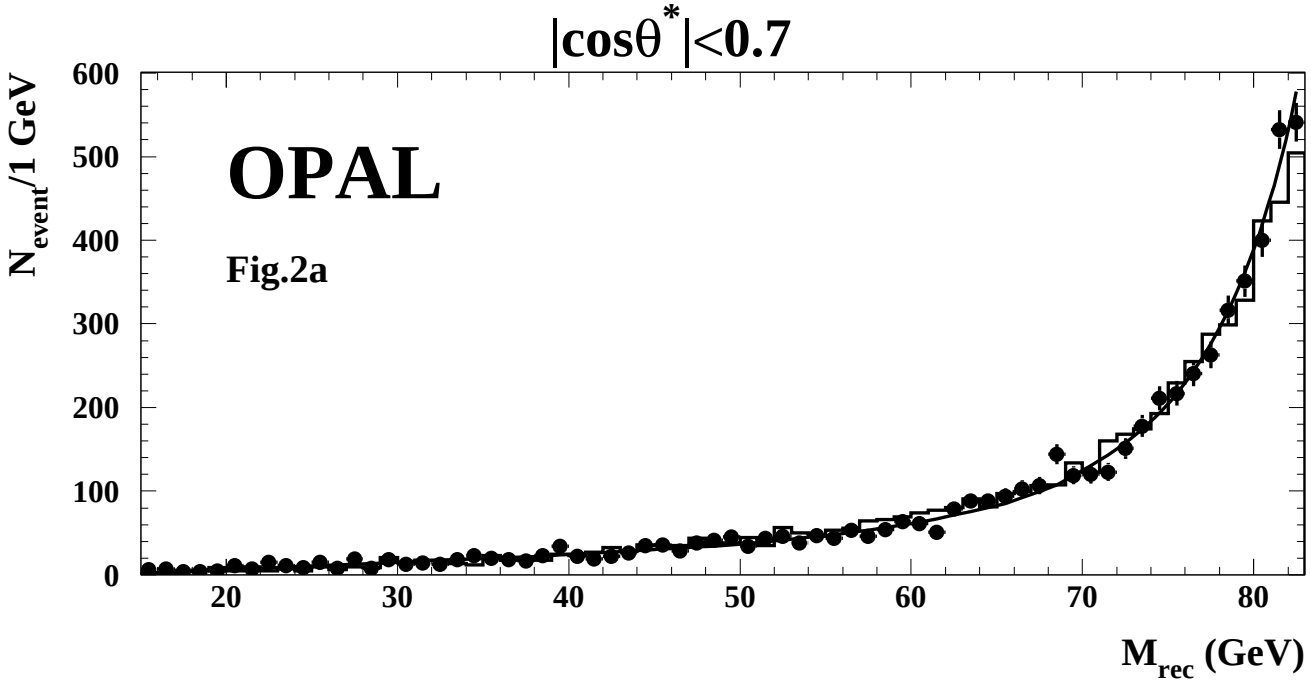
|cosθ*|<0.7
OPAL
Fig.2a
N_event/1 GeV
M_rec (GeV)

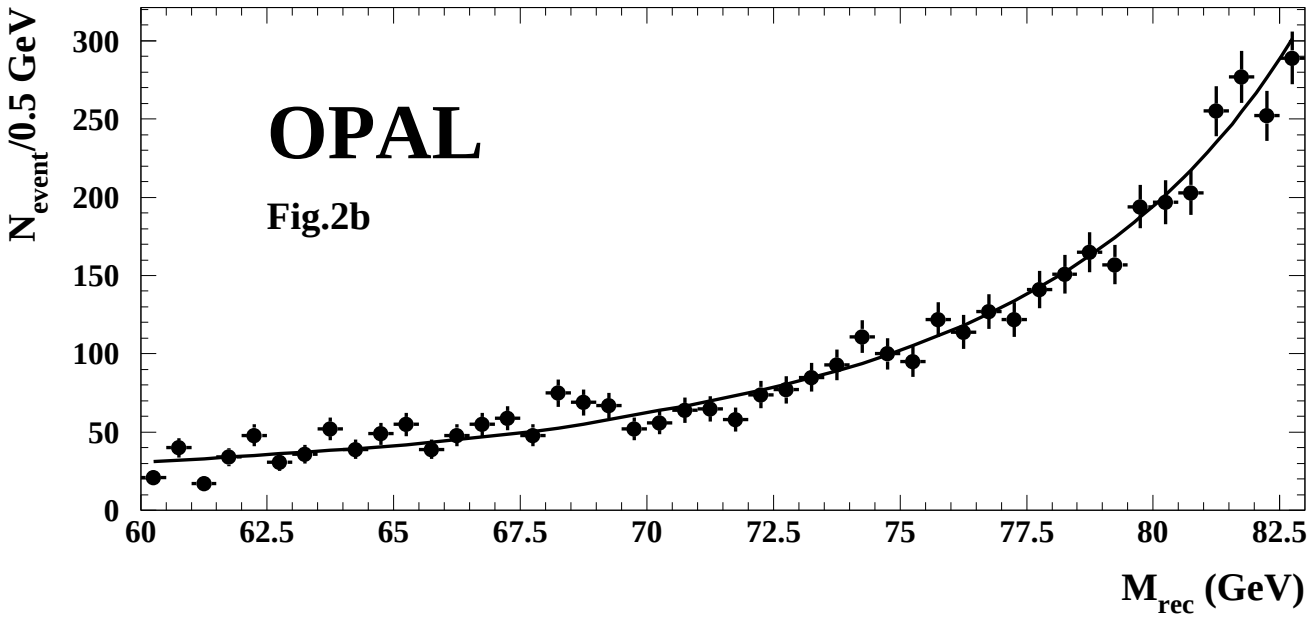
OPAL
Fig.2b
N_event/0.5 GeV
M_rec (GeV)

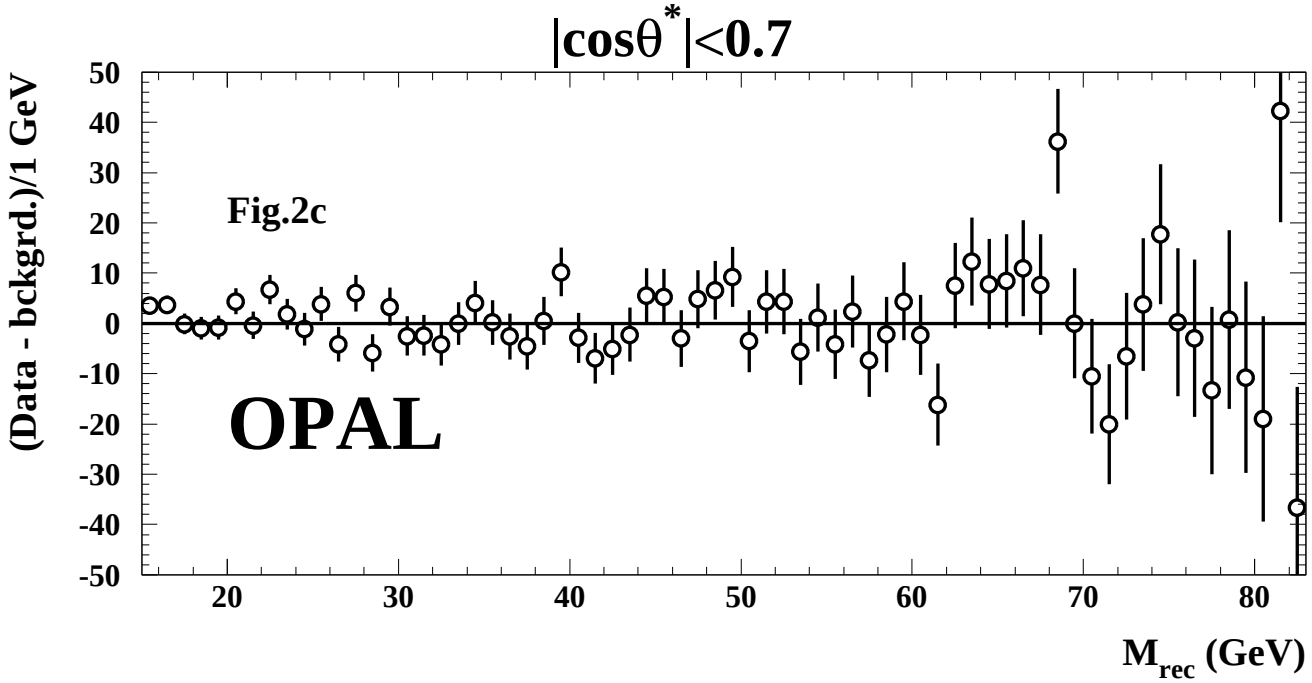
|cosθ*|<0.7
(Data - bckgrd.)/1 GeV
Fig.2c
OPAL
M_rec (GeV)

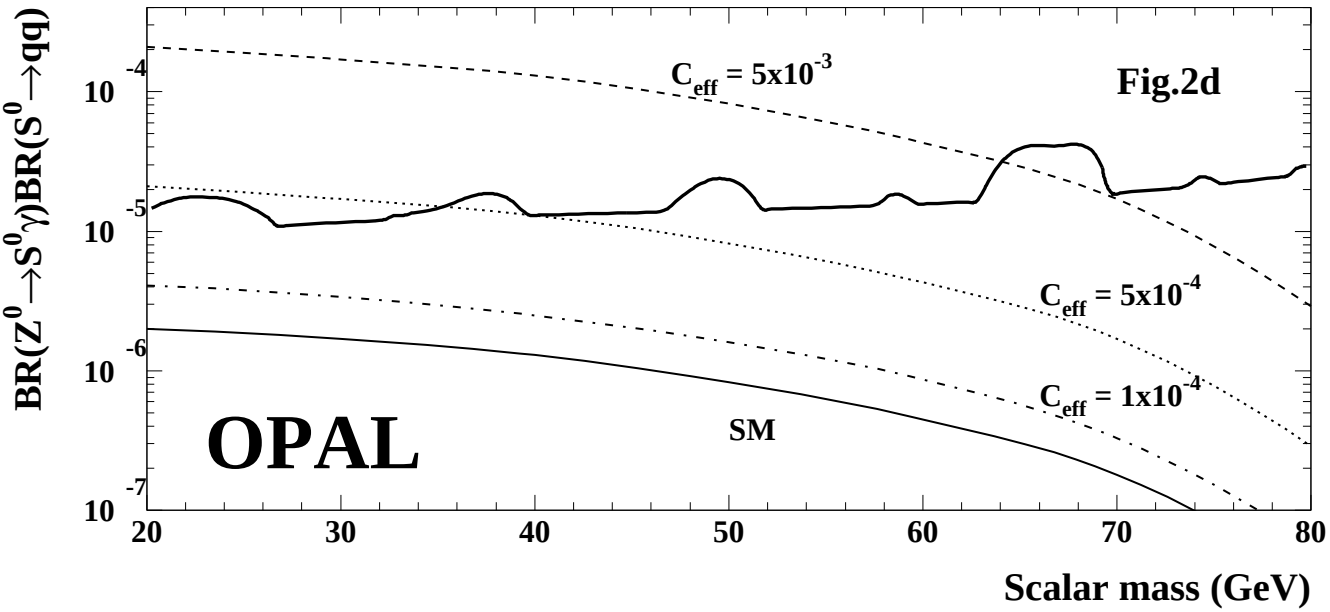
BR(Z⁰→S⁰γ)BR(S⁰→qq)
C_eff = 5x10⁻³
Fig.2d
C_eff = 5x10⁻⁴
C_eff = 1x10⁻⁴
SM
OPAL
Scalar mass (GeV)

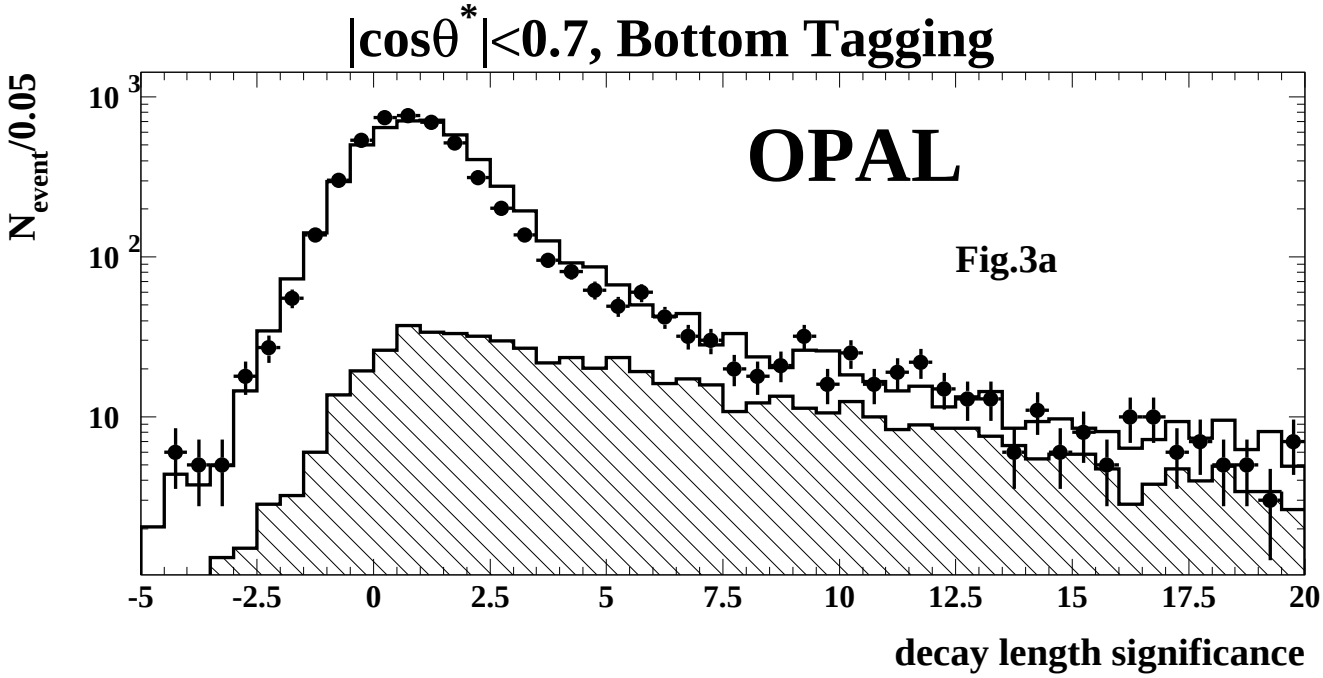
|cosθ*|<0.7, Bottom Tagging
OPAL
Fig.3a
N_event/0.05
10^3
10^2
10
-5
-2.5
0
2.5
5
7.5
10
12.5
15
17.5
20
decay length significance

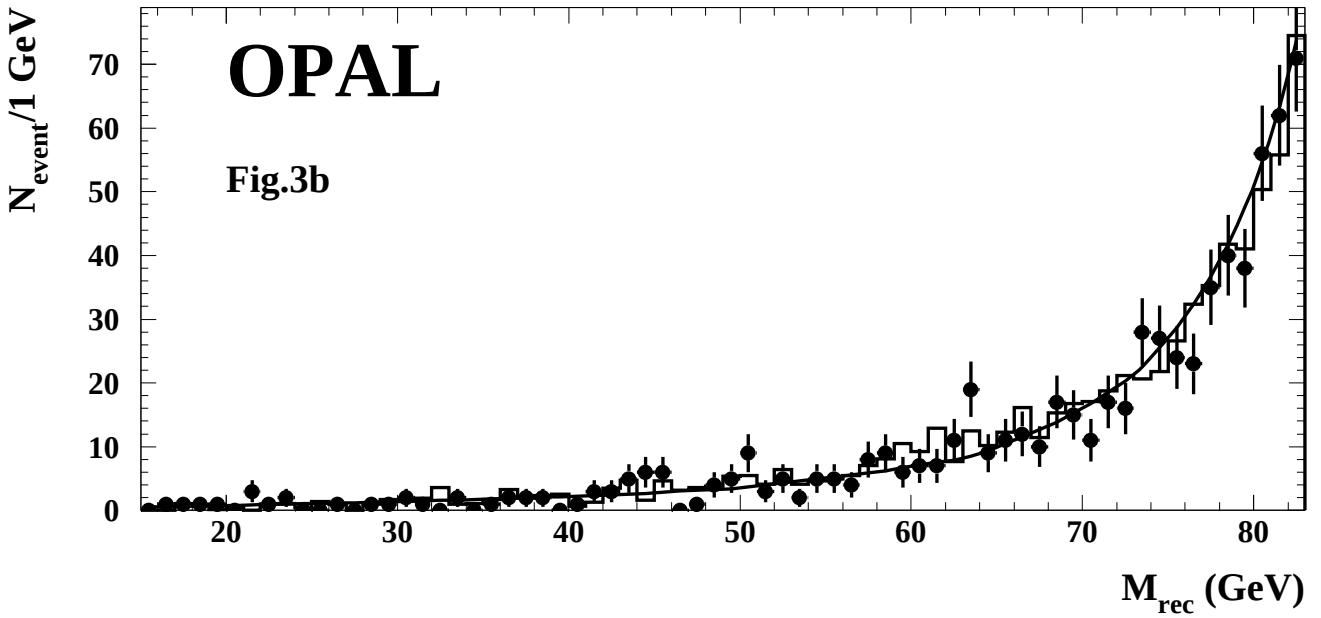
OPAL
Fig.3b
N_event/1 GeV
70
60
50
40
30
20
10
0
20
30
40
50
60
70
80
M_rec (GeV)

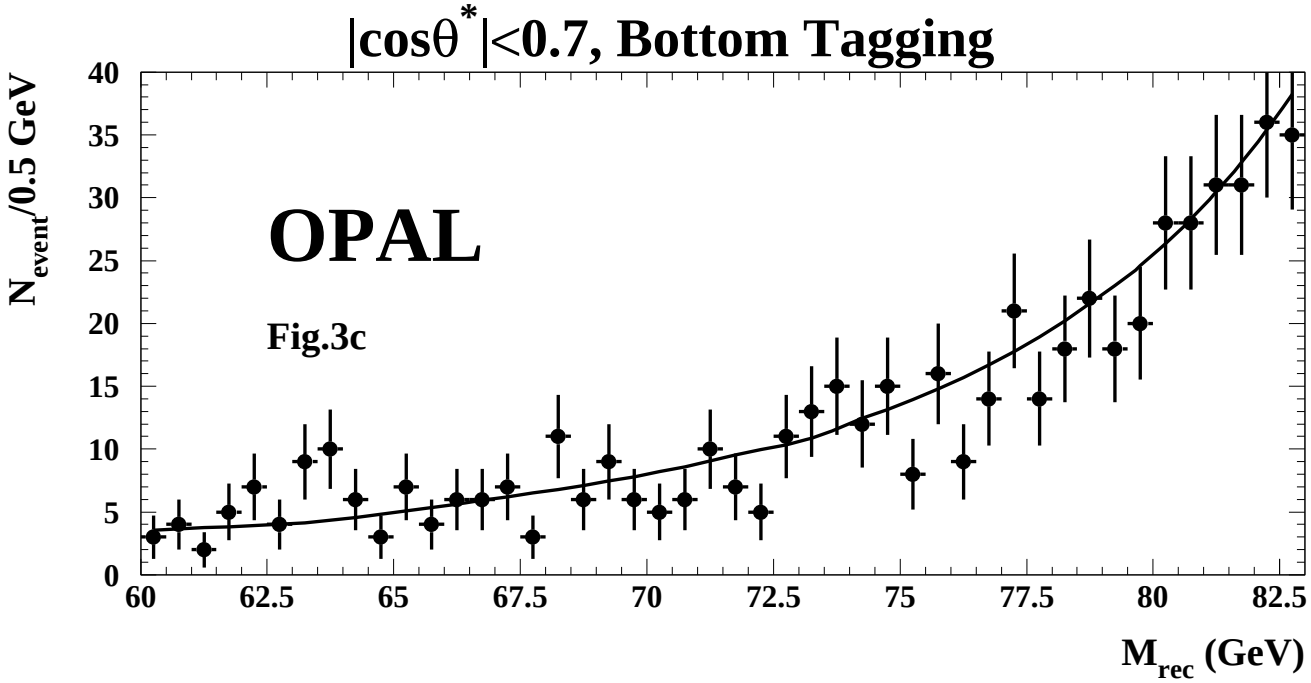
|cosθ*|<0.7, Bottom Tagging
OPAL
Fig.3c
N_event/0.5 GeV
M_rec (GeV)

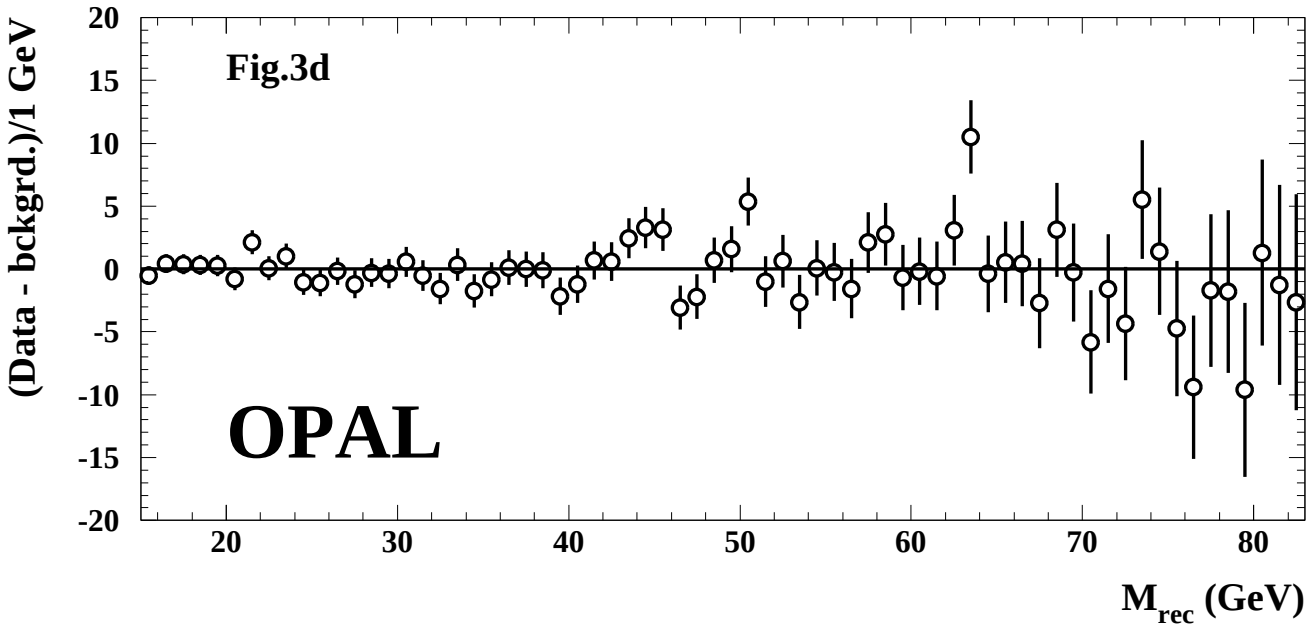
Fig.3d
OPAL
(Data - bckgrd.)/1 GeV
M_rec (GeV)

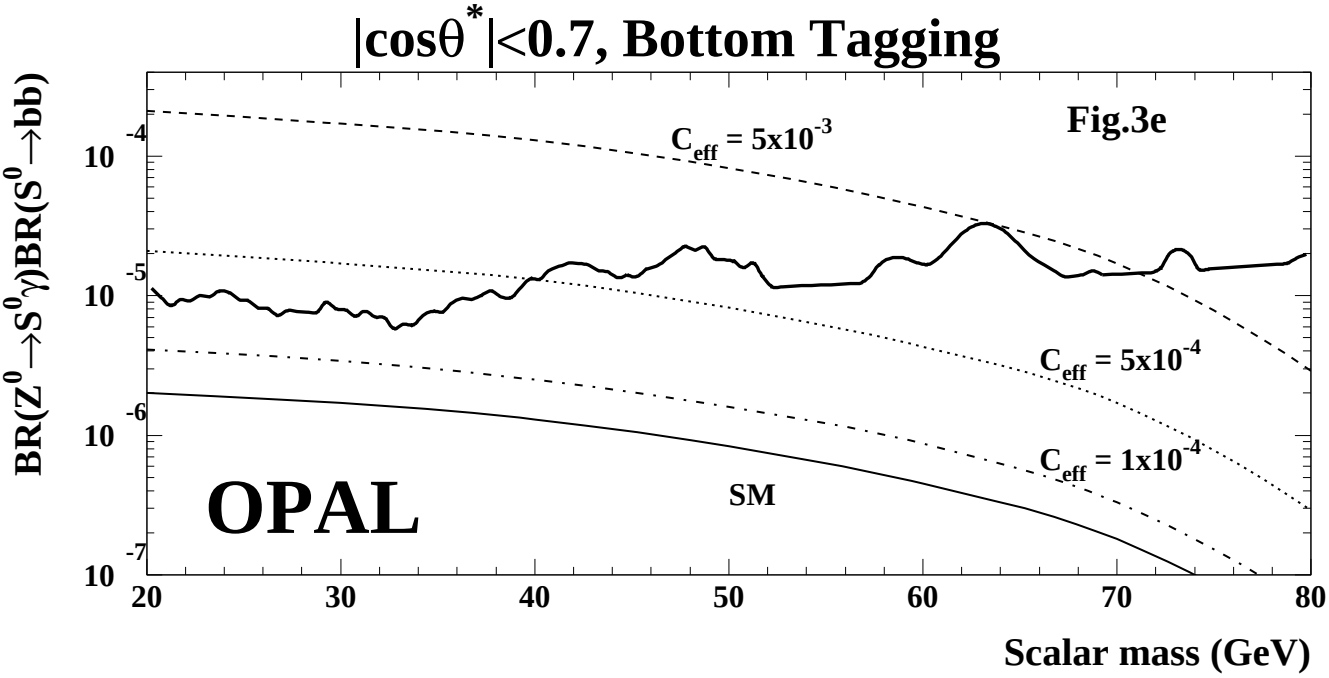
|cosθ*|<0.7, Bottom Tagging
Fig.3e
BR(Z⁰→S⁰γ)BR(S⁰→bb)
C_eff = 5x10⁻³
C_eff = 5x10⁻⁴
C_eff = 1x10⁻⁴
SM
OPAL
10⁻⁴
10⁻⁵
10⁻⁶
10⁻⁷
20
30
40
50
60
70
80
Scalar mass (GeV)

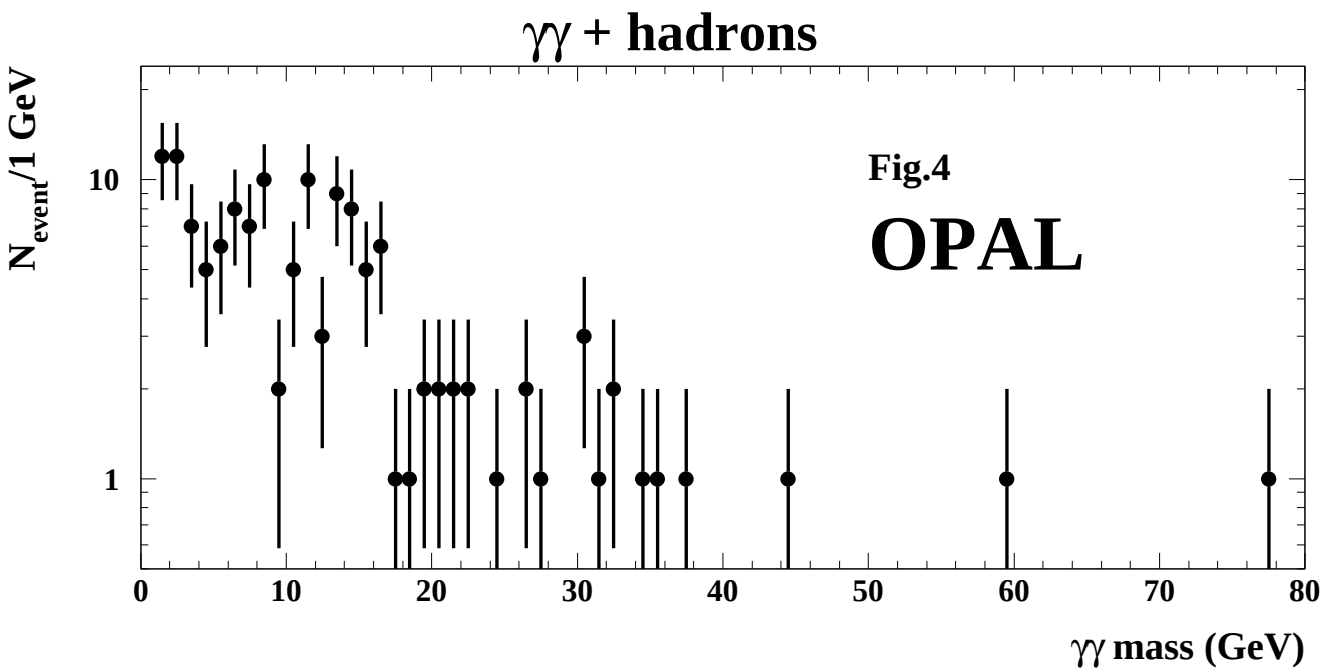
γγ + hadrons
N_event/1 GeV
10
1
0
10
20
30
40
50
60
70
80
γγ mass (GeV)
Fig.4
OPAL